Accepted Manuscript

Title: Metal organic framework (MOF) porous octahedral nanocrystals of Cu-BTC: Synthesis, properties and enhanced absorption properties

Authors: Ramanpreet Kaur, Amandeep Kaur, Ahmad Umar, William A. Anderson, Sushil Kumar Kansal

PII: S0025-5408(18)31125-5
DOI: https://doi.org/10.1016/j.materresbull.2018.07.025
Reference: MRB 10106

To appear in: *MRB*

Received date: 12-4-2018
Revised date: 17-7-2018
Accepted date: 20-7-2018

Please cite this article as: Kaur R, Kaur A, Umar A, Anderson WA, Kansal SK, Metal organic framework (MOF) porous octahedral nanocrystals of Cu-BTC: Synthesis, properties and enhanced absorption properties, *Materials Research Bulletin* (2018), https://doi.org/10.1016/j.materresbull.2018.07.025

Metal organic framework (MOF) porous octahedral nanocrystals of Cu-BTC: Synthesis, properties and enhanced absorption properties

Ramanpreet Kaur[1], Amandeep Kaur[1], Ahmad Umar,[2]* William A. Anderson[3] and Sushil Kumar Kansal[1*]

[1]Dr. S. S. Bhatnagar University Institute of Chemical Engineering & Technology, Panjab University, Chandigarh- 160014, India

[2]Department of Chemistry, Faculty of Science and Arts and Promising Centre for Sensors and Electronic Devices (PCSED), Najran University, Najran-11001, Kingdom of Saudi Arabia

[3]Department of Chemical Engineering, University of Waterloo, Waterloo, Canada

***Corresponding authors**

Prof. Sushil K Kansal

E-mail: sushilkk1@yahoo.co.in; sushilkk1@pu.ac.in

Tel/Fax: +91-0172-2534920/+91-172-2779173

Prof. Ahmad Umar

ahmadumar786@gmail.com (Ahmad Umar)

Phone: +966-534574597

Graphical abstract

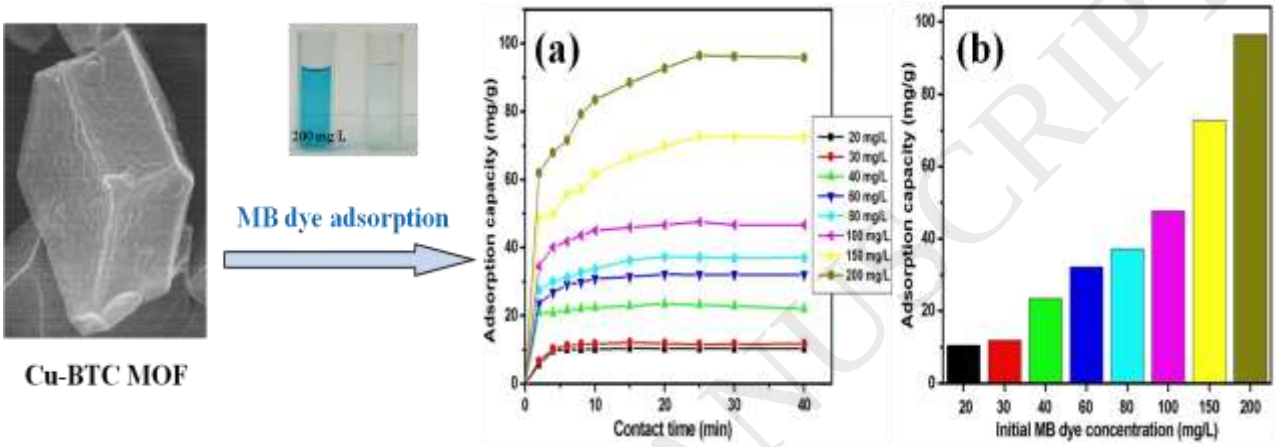

Highlights:

- Octahedral shaped Cu-BTC MOF was prepared using ultrasonic assisted hydrothermal method
- Cu-BTC was applied for the adsorption of MB dye
- Cu-BTC showed 96.4 mg/g equilibrium adsorption capacity

Abstract

Herein, we report the synthesis, characterization and enhanced absorption studies of porous octahedral shaped Cu-BTC (copper benzene-1,3,5-tricarboxylate) metal organic frameworks (MOFs). The Cu-BTC MOFs were synthesized by facile hydrothermal process and characterized by various techniques in order to examine the structural, morphological, thermal and adsorption-

desorption properties. The synthesized Cu-BTC MOFs were used as potential scaffold for the absorption of highly toxic azo dye, i.e. methylene blue (MB). Detailed absorption studies on the effect of initial pH, concentration, reaction time and temperature on adsorption of MB were analysed and it was observed that the removal of MB followed pseudo-2nd order kinetic model. Freundlich model fitted well as compared to Langmuir model with R^2 of 0.975 and thereby signifying a multilayer adsorption of MB on the surface of Cu-BTC MOFs. The observed maximal adsorption capacity for MB removal (200 mg/L) was ~ 101.21 mg/g using Langmuir isotherm. The Cu-BTC MOFs exhibited 42.3 mg/g adsorption capacity after fourth cycle of MB dye adsorption. These features exhibited that Cu-BTC MOF have potential for the adsorption of MB and can efficiently be used to treat wastewater.

Keywords: *Metal-organic framework, Cu-BTC, Methylene blue, Adsorption isotherm*

1. Introduction

With rapid industrialization and population growth, awareness of water pollution as a global threat has gradually increased and gained considerable attention worldwide [**1-5**]. Dyestuffs have become ubiquitous constitute of water pollution and are hazardous to the aquatic environment [**6-10**]. Dyes are mainly used in textile industry, however significant amount of dyes were utilized

to color several materials such as paper, leather, food and plastics. Dyes generally have xenobiotic basis and intricate aromatic structure that makes them highly stable to illumination, difficult to degrade and aerobic digestion [**11, 12**]. Their existence in water, even at minute concentration, is highly noticeable and unfavourable [**13, 14**]. It undergoes chemical and biological transformations in wastewater which decreases the oxygen solubility and thereby destroying aquatic life [**15, 16**]. Most of these dyes are highly dangerous for living creatures as they remain in the aquatic environment, degrading water quality and causing serious health ailments [**17-19**]. Therefore, the removal of these contaminants from wastewater is the need of the hour and to find effective ways to eliminate them completely is a major challenge.

Many treatment methods have been widely explored for the treatment of dyes containing water such as coagulation, photodegradation, ozonation, ultrafiltration and adsorption [**20, 21**]. Adsorption has been identified as an effective approach among these possible techniques owing to its high efficiency, economic feasibility and ease of operation [**22**]. However, the selection of efficient adsorbent is the imperative element for realistic use of adsorption technology [**23, 24**]. Many researchers have explored various adsorbents including clay material, biomass, activated carbon, zeolites, cellulose and other polymeric materials etc for the removal of dyes [**25-31**]. However, these adsorbents have low adsorption capacity and difficult to separate.

Over the last two decades, the field of porous coordination polymers has been growing remarkably. Metal organic frameworks (MOFs), a fascinating type of composite porous materials were first introduced by Yaghi and his co-workers. MOFs are fabricated by self association of metal clusters with organic linker, leading to the formation of framework structures. The fascinating properties make MOFs desirable for immense applications in gas separation, gas storage, catalysis, drug delivery, adsorption and energy storage [**32-37**]. MOFs are the potential candidates for the adsorption of dyes owing to their huge surface area, easy pore size tunability, and diversified morphology by linking with organic linkers and inorganic moieties [**38, 39**]. Moreover, the reports on adsorption behaviour for the removal of dyestuff from wastewater using MOFs are less explored. The treatment of wastewater containing methyl orange (MO) using MOF (Cr-BDC) was studied first time in 2010 [**40**]. Another study demonstrated that more sorption of benzene was achieved with MIL-101(Cr) than activated carbon owing to its high surface area and pore diameter [**41**]. Ma *et al.* prepared lignin based poly (acrylic acid)/organo-montmorillonite

composite using ultrasonic method and employed for the removal of Pb^{2+} ions. The adsorption mechanism for Pb^{2+} removal followed Freundlich isotherm [**42**]. Another study exhibited the effect of polymer loading in poly(acrylic acid) alumina composite for the adsorption of Pb^{2+} in aqueous phase. The nanocomposite with smaller poly(acrylic acid) loading showed higher Pb^{2+} absorption capacity. This may be attributed to less chocking of alumina pores by poly(acrylic acid). The adsorption kinetics followed pseudo second order equation [**43**]. Bakhtiari *et al.* fabricated MOF-5 using reflux method, exhibited cubic like morphology and used for the elimination of copper ions from water. The removal efficiency of copper ions enhanced with rise in temperature [**44**]. The application of MOF 235 (iron terephthalate) for the adsorption of harmful dyes such as methylene blue and methyl orange from contaminated water has also been reported. Cu-BTC is foremost explored MOF and recognized as HKUST which was initially described by Chui *et al.* in 1999 [**45**]. As far as, the majority of studies on Cu-BTC were focused on gas adsorption. Till now, there are few studies on the adsorption of dyes using Cu-BTC.

Here we report, synthesis of Cu-BTC using ultrasonic assisted hydrothermal method and then prepared MOF has been used for the adsorption of model compound i.e. MB, a cationic dye comes under azo group which is composed of nitrogen containing molecules. It is widely used in dying of wood, silk, cotton and also used as remedy for several diseases and disorders which includes methemoglobinemia, schizophrenia and urinary infections. However, it can cause nausea, eye burns, vomiting and chances of permanent damage to eyes of human and animals. Thus, the elimination of MB dye ions from wastewater is essential because of its toxicity. The objective of current work was to analyze the effect of reaction parameters such as pH, reaction time, MB dye concentration and temperature on adsorption process. The kinetic models and adsorption isotherms were assessed to examine the adsorption behaviour of MB dye on Cu-BTC MOF.

2. Experimental details

2.1. Materials

Methylene blue ($C_{16}H_{18}ClN_3S$, abbreviated as MB) from Merck company was used as the probe in this study. All the chemicals were used as delivered by company. Copper acetate monohydrate was bought from Merck, India and 1, 3, 5 benzene tricarboxylic acid (BTC) was

procured from Sigma-Aldrich. N, N-dimethylformamide (DMF) was supplied by Fisher scientific, USA while ethanol was obtained from Ultrapure, USA. DMF was used as solvent because of its ability to solubilise reactants, obtain highly crystalline materials and is favourable to construct porous structure in frameworks. In addition, it also participates in self assembly reactions of MOFs [**46**].

2.2. Synthesis of Cu-BTC MOF

The synthesis of Cu-BTC was done using ultrasonic assisted hydrothermal technique. Typically, 2.1014 g of 1,3,5 benzene tricarboxylic acid was mixed in 40 mL of mixture of methanol and N,N-dimethylformamide (1:1) and marked as solution I. Then, solution II was prepared by mixing 2.995 g of copper acetate monohydrate in 50 mL of mixture of ethanol/ distilled water (1:1). Both the solutions were separately stirred at ambient temperature for 30 minutes. After that solution I was added into solution II and sonicated for 30 minutes. Afterwards, the whole suspension was thermally treated in an autoclave for 20 hours at 393 K. The resulting blue product was separated and washed with DMF and ethanol several times. The collected product was dried in oven at 323 K for overnight and used for further experimentation.

2.3. Characterizations

The crystallinity and size of as-prepared sample was obtained by performing experiment on X-ray PANalytical model diffractometer. The structural characteristics, morphology and elemental composition were examined by taking images on FESEM and high resolution transmission electron microscope (FEI Technai F20 microscope) equipped with elemental analyzer. For FESEM and high resolution transmission electron microscopy (HRTEM) measurements, a known quantity of sample was dispersed in ethanol (organic solvent). All samples were extensively ultrasonicated for few hours to disperse the sample well. Fourier transform infrared (FTIR) spectrum was recorded on a Nicolet iS50 spectrophotometer (Thermoscientific, USA) with a scanning range of 4000-400 cm^{-1}. Thermal properties of sample were measured by carrying out TGA analysis on analytic instrument (Perkin-Elmer STA 6000) from temperature 0–600°C. Prior to the N_2 adsorption experiment, sample was degassed at 393 K for 6 hours. Specific surface area

was calculated based on adsorption desorption isotherm using Nova 2000e N_2-adsorption apparatus.

2.4. Adsorption capacity evaluation

The adsorption capacity of Cu-BTC MOF for MB removal was measured by conducting adsorption experiments. Stock solution of MB (200 mg/L) was made up and then diluted with double distilled water to prepare required concentrations of MB dye. The pH of dye solution was normalized with 1 M NaOH and 1 M HCl solutions. For adsorption experiments, 0.15 g adsorbent was suspended in constant volume of MB dye i.e. 100 mL in 250 mL of Erlenmeyer conical flask at 30 °C and at shaking rate of 175 rpm on an incubator shaker (KS 4000i model, IKA). The Cu-BTC was segregated from aqueous dye using Millipore syringe filter with a pore size of 0.45µm. The residual concentration of drug solution was recorded on UV-vis spectrophotometer. The adsorption capacity q_t (mg/g) was expressed as (1):

$$\text{Adsorption capacity } (q_t) = \frac{(C_0 - C_t)V}{m} \quad (1)$$

where, C_0 is the initial dye concentration and C_t is the dye concentration after adsorption at definite time (t). V is the volume of the MB solution that was taken and m is the weight of Cu-BTC. The effect of pH, initial dye concentration and temperature was examined for same dose of adsorbent at equilibrium time. The dilution of samples was done with double distilled water if the concentration values exceed the maximum absorption limit of calibration plot.

2.5. Desorption and recyclability properties

The regeneration of Cu-BTC MOF is important to reduce the cost of material. In present study, after completion of first adsorption cycle, the adsorbent was recovered through centrifugation for 10 min at rotation rate of 6000 rpm followed by washing carefully with ethanol solution until no methylene blue was identified. The recovered material was dried out at 50 ^{0}C in electric oven and reused for adsorption of MB dye solution (200 mg/L) for up to five adsorption cycles.

3. Results and discussion

3.1. Characterizations of Cu-BTC MOF

The powder X-ray diffraction (XRD) patterns were recorded to determine the crystal phase and structure of the sample. **Fig 1** represents the XRD pattern of Cu-BTC, in which characteristic peaks appeared at 2θ = 6.8°, 9.5°, 11.6°, 13.5°, 14.9°, 16.6°, 17.5°, 19.0°, 20.2°, 24.1°, 25.9°, 29.3°, 35.3° and 39.1° correspond to the (200), (220), (222), (400), (420), (422), (511), (440), (442), (551), (731), (751), (773) and (882) crystal planes respectively and are consistent with previous reported literature (Cambridge crystallographic information data with deposit number of 112954) [**47-51**]. The synthesized Cu-BTC exhibits similar intensity of characteristic peak (2θ =11.6°) for simulated Cu-BTC (inset of **Fig 1**), which confirms the high crystallinity of sample. No evident peak related to impurity was detected in the XRD patterns. The average crystallite size was estimated from Scherrer equation (2),

$$\mathbf{D = 0.9\lambda/FWHM\ Cos\ \theta}, \qquad (2)$$

where, λ is X-ray wavelength, FWHM is the angle width at the half maximum and θ is the Bragg's angle. The crystallite size of the Cu-BTC was found to be 79.54 nm.

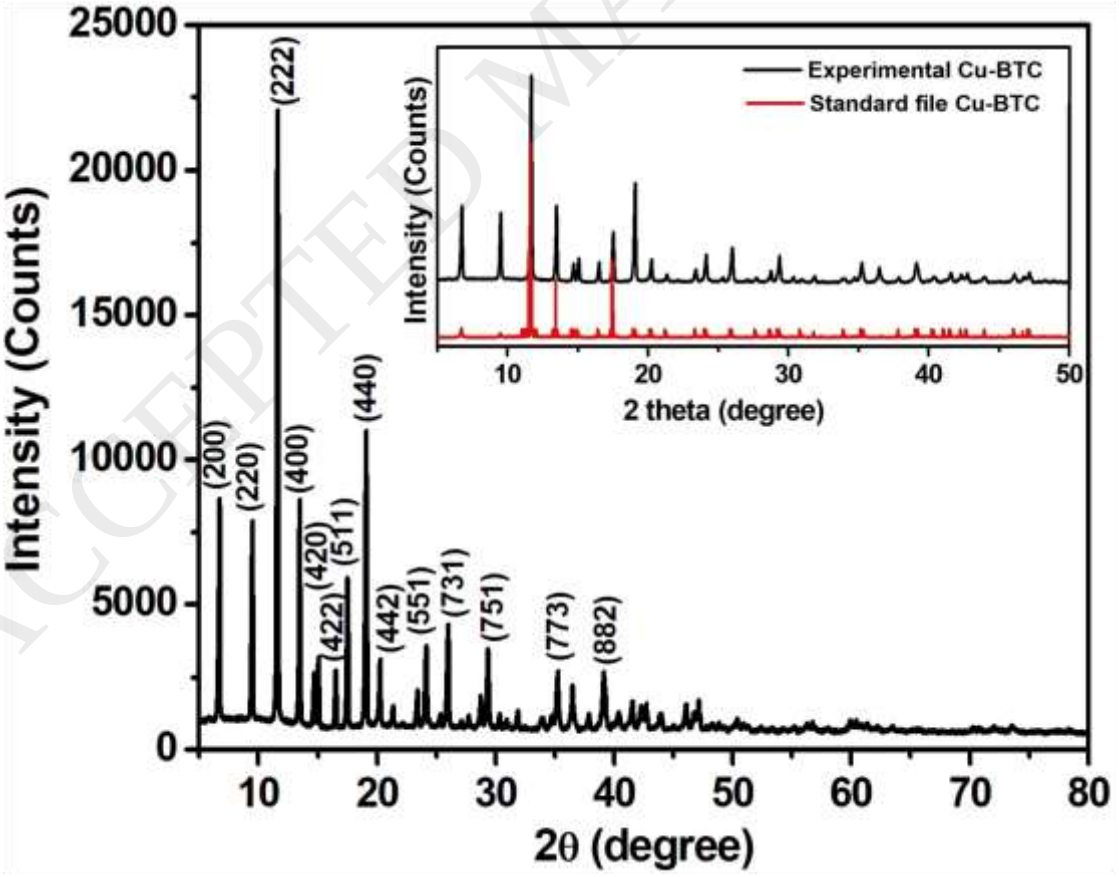

Fig. 1. XRD pattern of prepared Cu-BTC, (inset) Comparison of standard file with experimental XRD pattern of Cu-BTC

The morphology and the particles size of as-synthesized Cu-BTC was examined using TEM and FESEM analysis (**Fig. 2**). TEM images of Cu-BTC exhibit the accumulation of 0.2-0.5 μm crystals with well defined hexagonal (inset of **Fig 2**(a)) morphology in 2-dimensional. From **Fig 2**(c-d), the thickness of porous hexagonal crystals was about 1 nm, while it is impenetrable for electron beam and no clear lattice fringes were identified from HRTEM analysis (**Fig 2**(d)). In fact, as cleared from FESEM images (**Fig 2** (e and f)), the crystals of Cu-BTC exhibited octahedral shaped morphology.

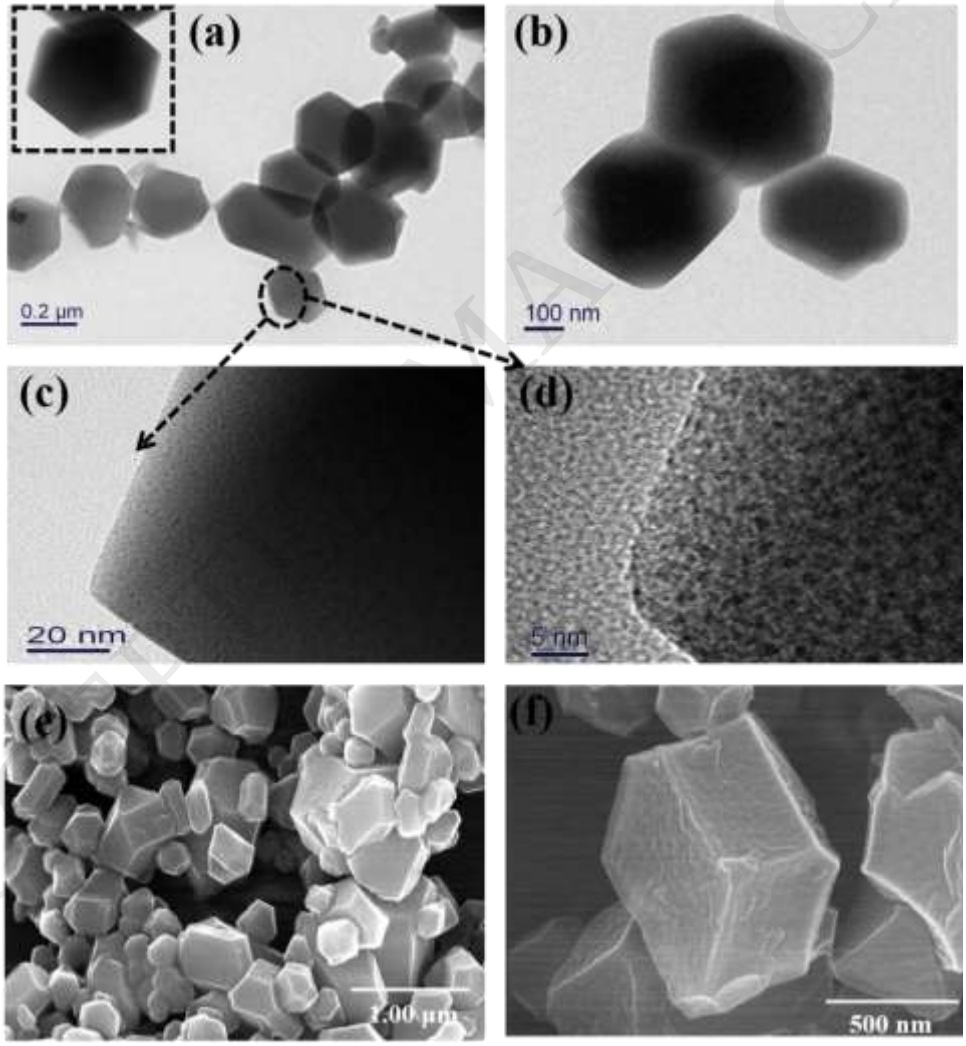

Fig. 2. Typical (a-d) TEM images, and (e-f) FESEM images of Cu-BTC

FTIR spectrum of Cu-BTC was recorded using KBr disks as shown in **Fig. 3**. The bands obtained at 488 cm^{-1} and 721 cm^{-1} may be due to the bending and stretching modes of Cu-O, respectively [**48, 52**]. The peaks observed between 663-766 cm^{-1} are assigned as ring in and out-of-plane bending vibration of aromatic ring. The adsorption bands appearing between 827-1153 cm^{-1} can be ascribed to symmetric and asymmetric stretching modes O−C=O and stretching vibrations of C−O of unreacted 1, 4 benzenedicarboxylic acid and reacted form of acid [**53**]. The strong absorption peaks at 1368, 1445 and 1640 cm^{-1} are related to the stretching mode of C-O, asymmetric and symmetric types of C=O, respectively [**39, 54**] It is imparting to the reaction of -COOH group (in 1, 3, 5-benzenetricarboxylic acid) with Cu ions. The small peak at 2933 cm^{-1} is due to DMF, while this peak does not exist where samples are exchanged with methanol [**55**]. The broad band appearing at 3346 cm^{-1} is associated to the surface-sorbed water and hydroxyl groups in the Cu-BTC structure [**56, 57**].

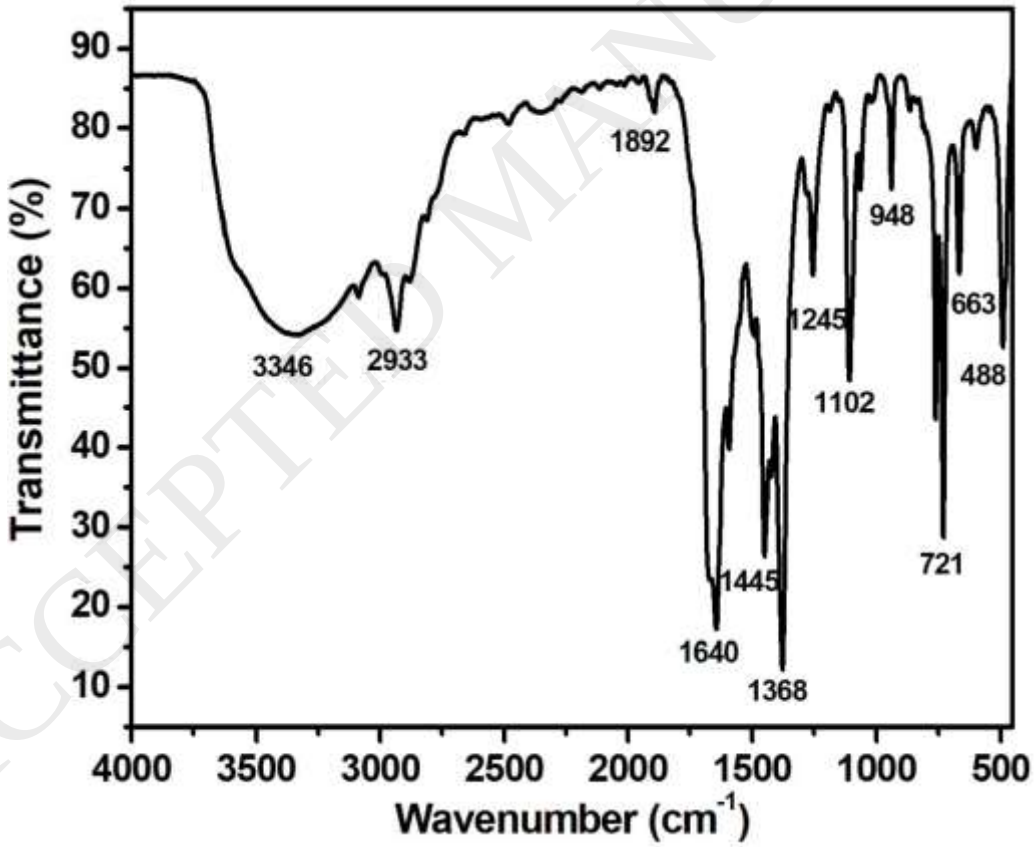

Fig. 3. Typical FTIR spectrum of Cu-BTC

The thermal properties of as-prepared sample were examined on TGA-DTG instrument and their results are shown in **Fig. 4** (a). The prominent weight loss occurred in the range of 40 ^{0}C

to 380 ^{0}C with three DTG peaks at 51 ^{0}C, 165 ^{0}C and 350 ^{0}C. The first weight loss of about 7.8% up to 100 ^{0}C corresponds to the removal of adsorbed water and ethanol. The second step of mass loss was about 55.8 % in the temperature range of 100 ^{0}C to 380 ^{0}C is due to the evaporation of DMF and oxidation of trimesic acid linkers and formation of CuO as end product [**58, 59**]. DSC experiment (**Fig. 4**(b)) has been performed to examine the thermal changes in the sample. The Cu-BTC exhibits endothermic band at 54 ^{0}C, 281 ^{0}C which correspond to the elimination of water, ethanol and DMF solvent. In comparison, exothermic peak obtained at 360 ^{0}C shows the thermal decomposition of Cu-BTC to CuO and Cu_2O, respectively. This thermal stability is identical to the study that is given by Liang *et al*., [**60**].

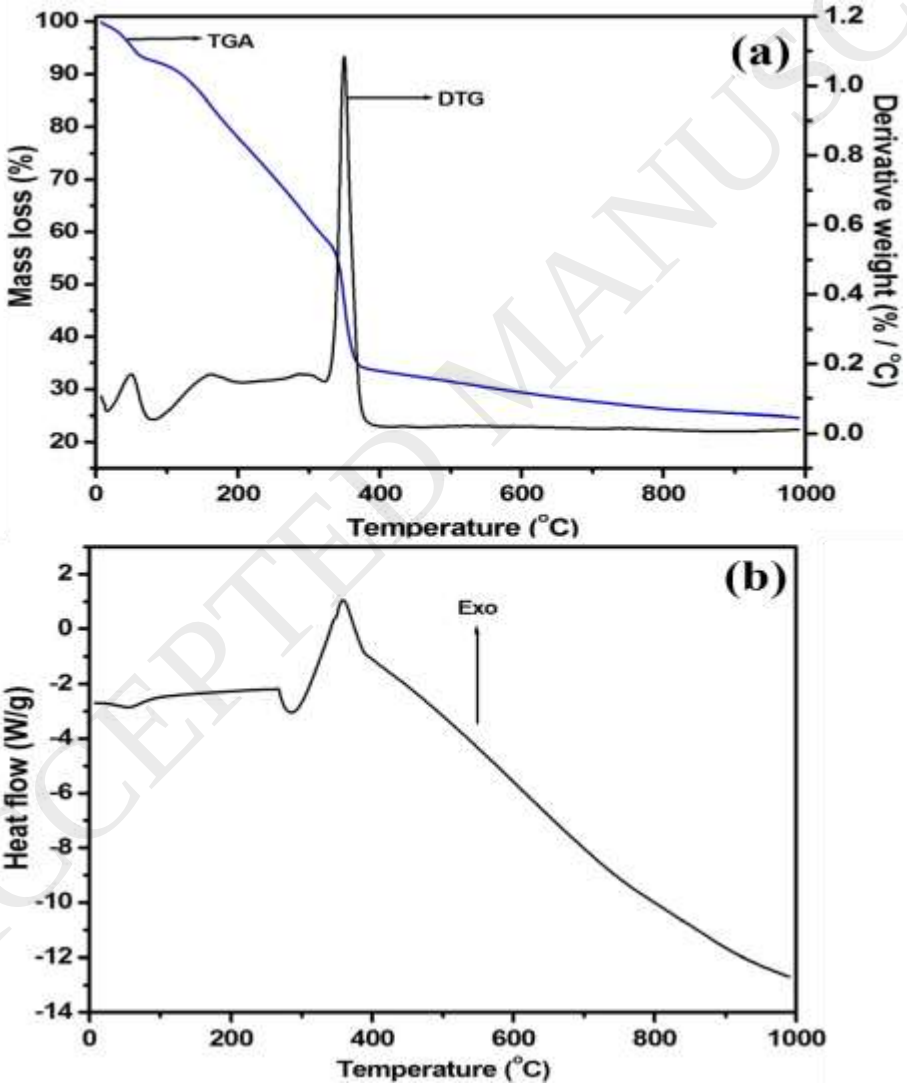

Fig. 4. Typical (a) TGA-DTG and (b) DSC curve of Cu-BTC

N_2 adsorption-desorption isotherm was obtained to find out specific surface area and pore volume of Cu-BTC and related results are illustrated in **Fig. 5**. The as-prepared Cu-BTC displays a type-IV IUPAC isotherm, indicating the existence of mesoporous materials and similar results are given by Lin *et al* [**54**]. The pore size distribution of sample was estimated from adsorption curve of isotherm by using Density Functional Theory (DFT) method with an average diameter of 2.44 nm and specific surface area (S_{BET} = 520.87 m^2/g, $S_{Langmuir}$ = 763.40 m^2/g). Total pore volume was found to be 0.3180 cc/g for pores half width less than 66.81 nm at P/P_0 = 0.98542.

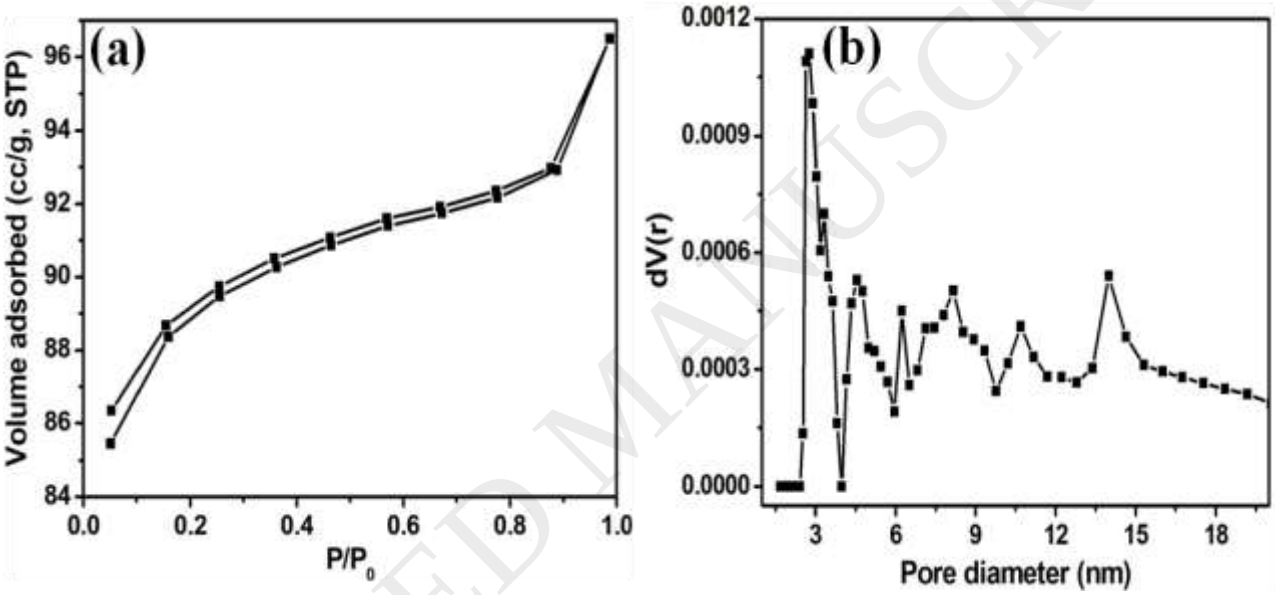

Fig. 5. (a) N_2 adsorption-desorption isotherm (b) DFT (Density Functional Theory) pore size distribution of synthesized Cu-BTC

3.2. Effect of pH on adsorption of methylene blue

To examine the effect of pH on adsorption of methylene blue (10 mg/L) onto Cu-BTC surface, a set of adsorption experiments (**Fig. 6**) were done in the pH range from 2-11 with adsorbent dose of 1.5 g/L at constant temperature (25 ^{0}C). The pH of suspension was regulated by adding 1 M NaOH and 1 M HCl. It is a crucial parameter that controls the adsorption process by measuring equilibrium adsorption capacity. The adsorption capacity (mg/g) increases with increase in pH from 2 to 7 (Fig. 4.7(a)). At lower pH, surface of Cu-BTC gets positively charged, thus making H+ ions to compete with dye cations causing a decrease in the amount of adsorption.

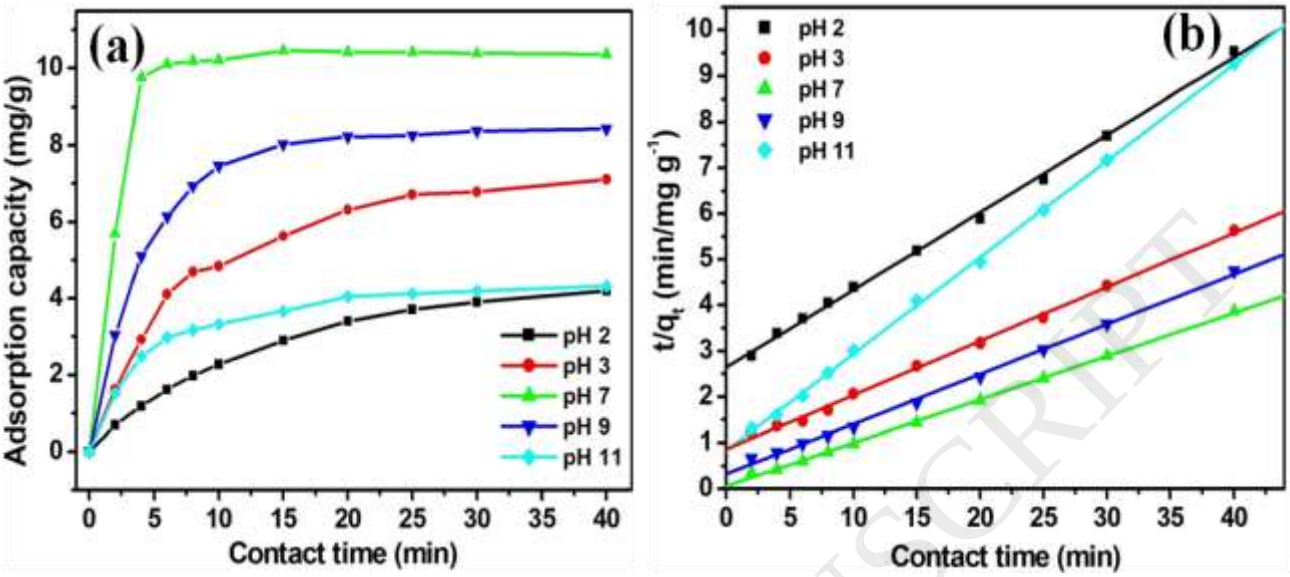

Fig. 6 Effect of initial pH on (a) adsorption capacity after equilibrium time (40 min), (b) pseudo second order kinetics. Experimental conditions: (C_0 = 20 mg/L, adsorbent dose = 1.5 g/L, r (rate) = 175 rpm, T = 25 ˚C)

However, the adsorption capacity was decreased from 10.45 mg/g to 4.32 mg/g with increase in pH from 7 to 11. At higher pH, MB containing chlorine anions react with NaOH to produce NaCl and MB-S^+ OH (aqueous) through displacement reaction. The amount of NaCl salt can decrease the adsorption of MB-S^+ OH (aqueous) on adsorbent surface [**61, 62**]. Moreover, it was cleared that maximum removal efficiency and adsorption capacity reached to 97.6 % and 10.45 mg/g at pH 7. As a result, pH 7 was chosen as optimum pH for further experiments. Moreover, the point of zero charge for Cu-BTC was found to be 4.0. At pH ≥4.0, the surface of adsorbent turned negatively charged and it is positively charged below pH ≤ 4.0. Therefore, the adsorption of methylene blue onto Cu-BTC is favored for when pH ≥ $pH_{ZPC,}$ but is unfavourable for pH ≤ pH_{ZPC} [**63, 64**]. The data for the adsorption of MB dye over Cu-BTC followed pseudo-2^{nd} order kinetic model (**Fig. 6**(b)).

3.3. Effect of contact time and initial concentration

Fig. 7 (a) displays the effect of contact time on adsorption capacity. It was observed that adsorption of MB on Cu-BTC increased gradually at beginning of reaction. Afterwards, the

adsorption goes stagnant till equilibrium was attained. The optimal MB adsorption was acquired during initial period of adsorption and finally attained equilibrium after 20 minutes and 30 minutes for 20-80 mg/L and 100-200 mg/L, respectively. After that an increase in reaction time showed minor changes in the adsorption capacity. Maximum adsorption in the beginning is attributed to the availability of vacant adsorption sites of Cu-BTC adsorbent which provides accommodation for dye ions. But as the adsorption continues for extended period of time, the active sites gets occupied with dye ions and therefore repulses the remaining MB ions from bulk to surface of adsorbent thereby decreasing the removal efficiency. Therefore, contact time of 40 minutes (96.4 mg/g adsorption capacity for 200 mg/L MB solution) was opted for the subsequent works.

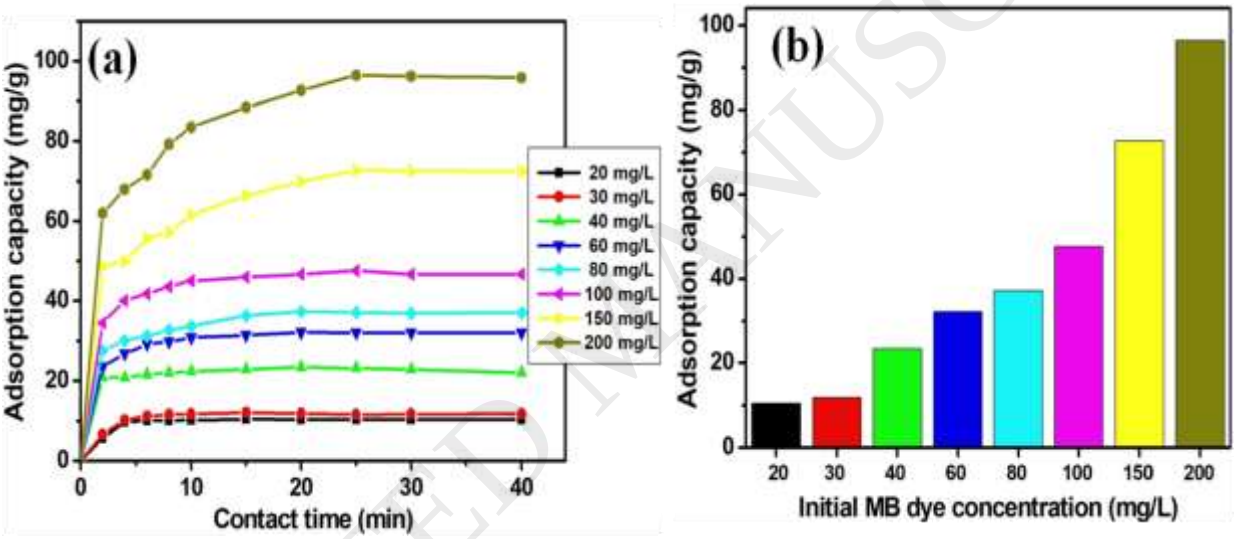

Fig. 7. Effect of (a) contact time (b) initial concentration on the adsorption capacity of Cu-BTC, Experimental conditions: (adsorbent dose = 1.5 g/L, r (rate) = 175 rpm, T = 298 K)

The effect of initial dye concentration on MB adsorption was investigated by altering the dye concentrations from 20 to 200 mg/L, keeping other parameters constant, i.e. dye solution 100 mL, pH 7 and temperature 298 K. The adsorption capacity of MB was enhanced from 10.5 to 96.4 mg/g as MB concentration increased from 20 to 200 mg/L (**Fig. 7** (b)). This is possibly owing to higher concentration gradient i.e. at higher initial dye concentration, which helps in better mass transfer between solid (adsorbent) and liquid (adsorbate) phases [**65**].

3.4. Effect of temperature

The effect of temperature on adsorption capacity of MB dye (200 mg/L) was investigated by performing the experiments at three different temperatures i.e. 298 K, 308 K and 318 K. **Fig. 8** exhibits that amount adsorbed on the surface of Cu-BTC declined with rise in temperature thus signifying the exothermic nature of the adsorption process. The adsorption capacity of Cu-BTC for MB (200 mg/L) was found to decrease from 95.8 mg/g to 82.5 mg/g as temperature increases from 298 K to 318 K. (**Fig. 8**).

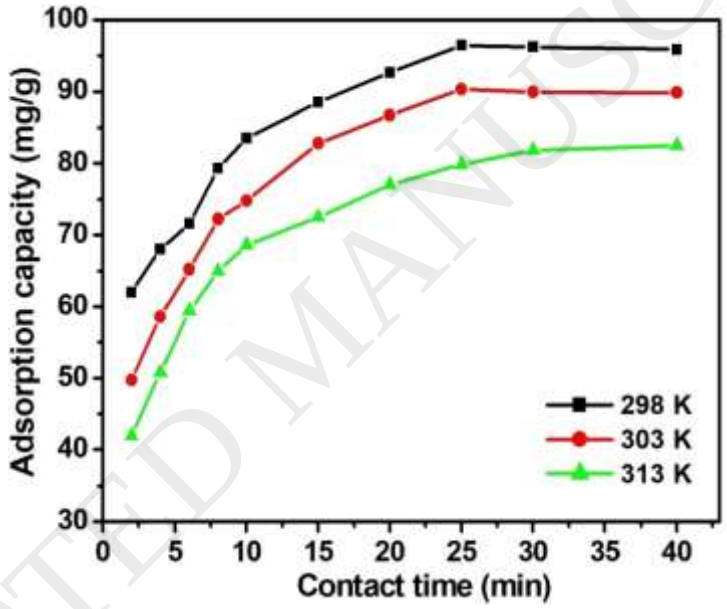

Fig. 8. Effect of temperature on amount adsorbed of MB dye (200 mg/L) over Cu-BTC (contact time = 40 min, shaking speed = 175 rpm, pH= 7, and adsorbent dose = 0.15 g).

3.5. Kinetic study

To get insight of potential reaction mechanism, the theoretical kinetic models were studied by analyzing the changes in adsorptive capacity against time. The kinetics of adsorption of MB onto Cu-BTC was explored using pseudo-first-order and pseudo-second order and intra-particle diffusion respectively. The equation of pseudo-first-order kinetic model (3) can be described as [**66**]:

Pseudo-1st order kinetic model, $\log(q_e - q_t) = \log q_e - \frac{k_1}{2.303} t$ (3)

where k_1 (min^{-1}) is pseudo-1st order rate constant, q_e (mg/g) is equilibrium adsorption, q_t (mg/g) is adsorption capacity at time't'. The rate constant k_1 for different dye concentrations were estimated from the slope of the plot of $\log(q_e-q_t)$ versus contact time (**Fig. 9**(a)). The plots seem to maintain linearity upto some extent for different initial dye concentrations i.e. 20-200 mg/L. The coefficient of correlation (R^2) was calculated to be high (near to 1), but adsorption capacity values were inconsistent with calculated values (**Table 1**). This depicts that this model is relatively inappropriate for showing kinetic adsorption data.

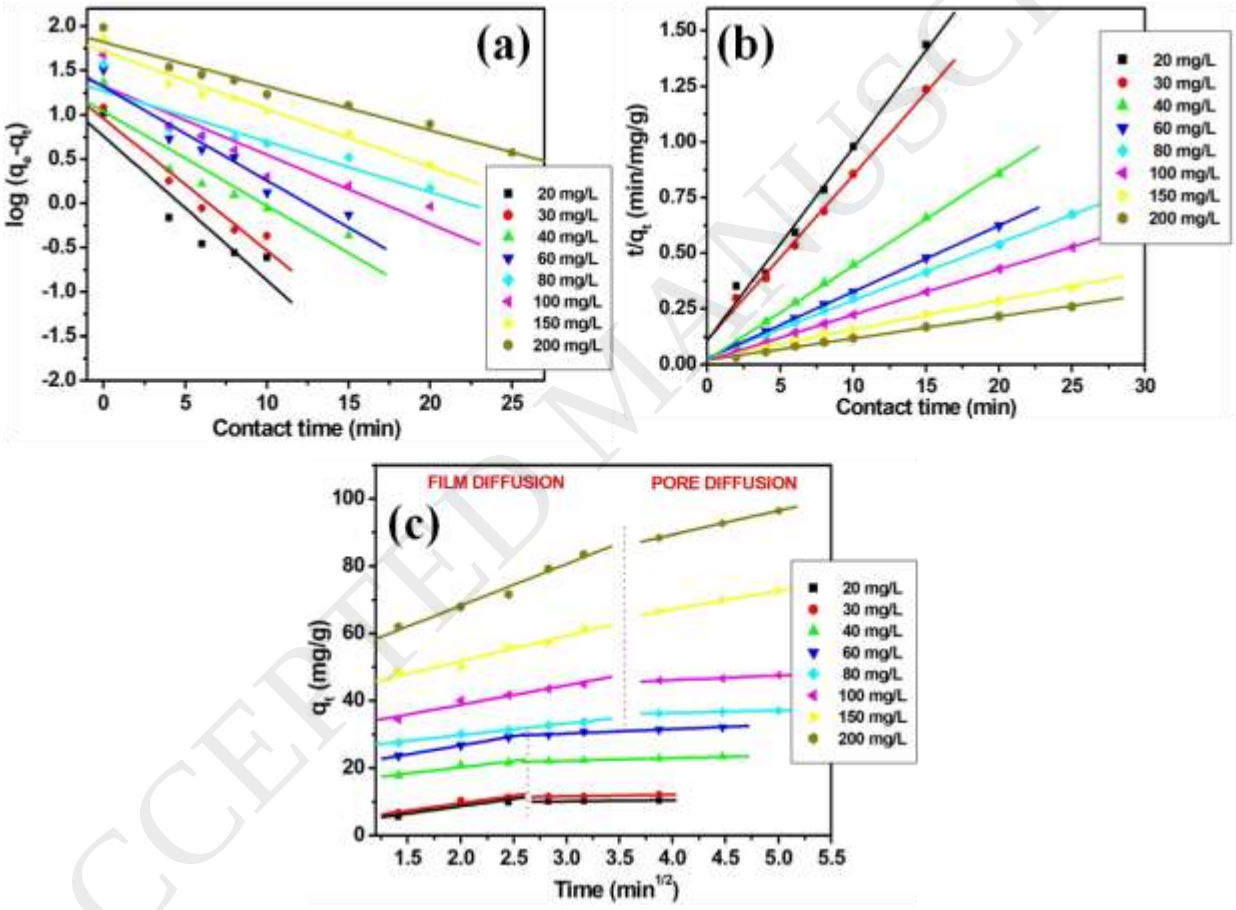

Fig. 9. (a) pseudo-1st order (b) pseudo-2nd order (c) intra-particle-diffusion plot for the adsorption of MB dye over Cu-BTC

In order to study the goodness of fit for 2nd order kinetic model, experiments were carried out at different dye concentrations. The pseudo-2nd order kinetic model can be described by following equation (4) [**67**]:

$$\frac{t}{q_t} = \frac{1}{k_2 q_e^2} + \frac{t}{q_e} \quad (4)$$

where k_2 (min g/mg) is pseudo-2nd order rate constant, which can be determined from the plot of t/q_t and contact time (**Fig. 9**(b)). The plots for all dye concentrations showed good linearity over period of contact time and correlation coefficient (R^2) values close to 1 for second order kinetic model. In addition, similar values for experimental and calculated adsorption capacity (Table 1) showed the suitability of this model for the adsorption.

The importance of intra-particle diffusion model for adsorption study is to determine the rate limiting step for adsorption process and was stated by Weber and Morris [**68**]. Moreover, this model also gives the idea about the probability of pore diffusion of the dye ions from liquid phase (bulk) into the solid phase. So, in order to study the probable pore diffusion method and rate controlling steps, it could be explained in terms of Fick's second law and linearized intra particle diffusion equation was described using following equation:

$$q_t = k_{id}\, t^{1/2} + C \quad (5)$$

where parameter, k_{id} (mg/g min$^{0.5}$) is the rate constant for intraparticle diffusion and C is the intercept that is calculated from plot of q_t versus $t^{1/2}$ (**Fig. 9**(c)) and parameters are given in Table 1. Fundamentally, if the graph shows straight line and passes through origin, then adsorption is influenced by intra-particle diffusion but if the plot does not maintain linearity then the film diffusion process is rate limiting step. In this study, data obtained for intra-particle diffusion at different dye concentrations appear to split into two main regions. The first data fits at initial time period shows external mass transfer which includes the movement of dye ions from aqueous solution to solid periphery of the adsorbent. The second data fit indicates slow adsorption phase which is influenced by pore diffusion method. Therefore, it can be inferred that intra-particle diffusion occurs, but it is not the rate determining step since the best fit does not passes through the origin. Overall, it is clear that present adsorption process is very complicated and both diffusion types dominate the rate of adsorption process.

Table 1. Kinetic parameters for the adsorption of methylene blue (MB) using Cu-BTC

Pseudo-first-order	**20 mg/L**	**30 mg/L**	**40 mg/L**	**60 mg/L**	**80 mg/L**	**100 mg/L**	**150 mg/L**	**200 mg/L**
k_1 (min^{-1})	0.376	0.344	0.246	0.244	0.132	0.179	0.149	0.114
$q_{e(exp)}$ (mg/g)	10.5	12.1	23.3	32.1	37.1	47.6	72.7	96.4
$q_{e(cal)}$ (mg/g)	5.8	9.1	10.9	20.8	18.7	21.2	51.5	65.9
R^2	0.9254	0.9734	0.9296	0.9655	0.9157	0.9299	0.9813	0.9859
Pseudo-second-order	**20 mg/L**	**30 mg/L**	**40 mg/L**	**60 mg/L**	**80 mg/L**	**100 mg/L**	**150 mg/L**	**200 mg/L**
k_2 (g/mg/min)	0.07	0.049	0.079	0.032	0.020	0.021	0.006	0.005
$q_{e(exp)}$ (mg/g)	10.5	12.1	23.3	32.1	37.1	47.6	72.7	96.4
$q_{e(cal)}$ (mg/g)	11.5	13.4	23.7	33.5	39.1	49.1	77.6	102.8
R^2	0.9944	0.9976	0.9997	0.9999	0.9994	0.9999	0.9978	0.9986
Intra-particle diffusion	**20 mg/L**	**30 mg/L**	**40 mg/L**	**60 mg/L**	**80 mg/L**	**100 mg/L**	**150 mg/L**	**200 mg/L**
$k_{id,1}$ ($mg/g/min^{0.5}$)	4.40	4.44	3.73	5.43	3.45	5.80	7.52	12.40
C_1	0.09	0.74	12.8	15.8	22.9	27.2	36.8	43.5
R^2	0.9293	0.9676	0.96841	0.9999	0.9970	0.9778	0.9704	0.9877
$k_{id,2}$ ($mg/g/min^{0.5}$)	0.28	0.49	0.79	1.32	0.72	1.39	5.54	7.03
C_2	9.4	10.2	19.77	26.3	33.5	40.6	45.0	61.2
R^2	0.9775	0.983	0.9963	0.9662	0.9996	0.9910	0.9994	0.9999

3.6. Adsorption isotherm study

Adsorption isotherm gives explanation of interaction between dye ions and adsorbent, and also help in optimizing the adsorbent at distinct process variables. The equilibrium data was estimated from the optimal adsorption capacity of Cu-BTC for the removal of dye ions and was further modeled with Langmuir, Freundlich and Temkin models (**Fig. 10 (a-c)**) and data given in Table 1 [**55**]. The Langmuir model represents monolayer molecular adsorption which occurs on a

homogeneous surface, whereas Freundlich model is usually applicable for multilayer adsorption which takes place on a heterogeneous surface. The Temkin isotherm model contains a factor that explicitly shows adsorbate- adsorbent interactions, it is assumed that heat of adsorption of all molecules in the layer would decrease linearly rather than logarithmic with adsorption [**69**]. The Langmuir adsorption isotherm equation may be written as:

$$\frac{C_e}{q_e} = \frac{1}{q_L b} + \left(\frac{1}{q_L}\right) C_e \quad (6)$$

where q_L (mg/g) is monolayer adsorption capacity, b (L/mg) is Langmuir isotherm constant, q_e (mg/g) is the amount of MB adsorbed at equilibrium, C_e (mg/L) is the equilibrium concentration of MB. The plot (**Fig. 10 (a)**) of (C_e/q_e) against C_e gives a straight line if adsorption equilibrium follows Langmuir isotherm. For anticipating the favorability of an adsorption, the dimensionless separation factor based on Langmuir equation was used. R_L separation factor can be expressed as follows:

$$R_L = \frac{1}{1 + bC_0} \quad (7)$$

where, R_L value signifies the favorability and ability of the adsorption system. When R_L value lies between 0 and 1, it shows good adsorption. The Freundlich isotherm equation may be written as:

$$\ln q_e = \ln K_f + \frac{1}{n} \ln C_e \quad (8)$$

where K_f (mg/g) is the Freundlich constant, n is the adsorption constant, the value of 1/n in the range of 0.1 to 1 represents a favorable adsorption. The value of 1/n (Table 2) for all concentrations has less than 1 confirms the favorability of adsorption.

The linearized form of Temkin isotherm equation can be written as:

$$q_e = B_1 \ln K_T + B_1 \ln C_e \quad (9)$$

where $B_1 = RT/b_T$, K_T is the equilibrium constant (L/mg) at optimum binding energy, B_1 is the constant corresponding to heat of adsorption (J/mol). The constant parameters of plot (**Fig. 10** (c)) are given in **Table 2**. As shown in **Fig. 10**, it was clear that correlation coefficient (R^2) fitted better with Freundlich isotherm (R^2 = 0.97527) as compared to Langmuir and Temkin isotherm models.

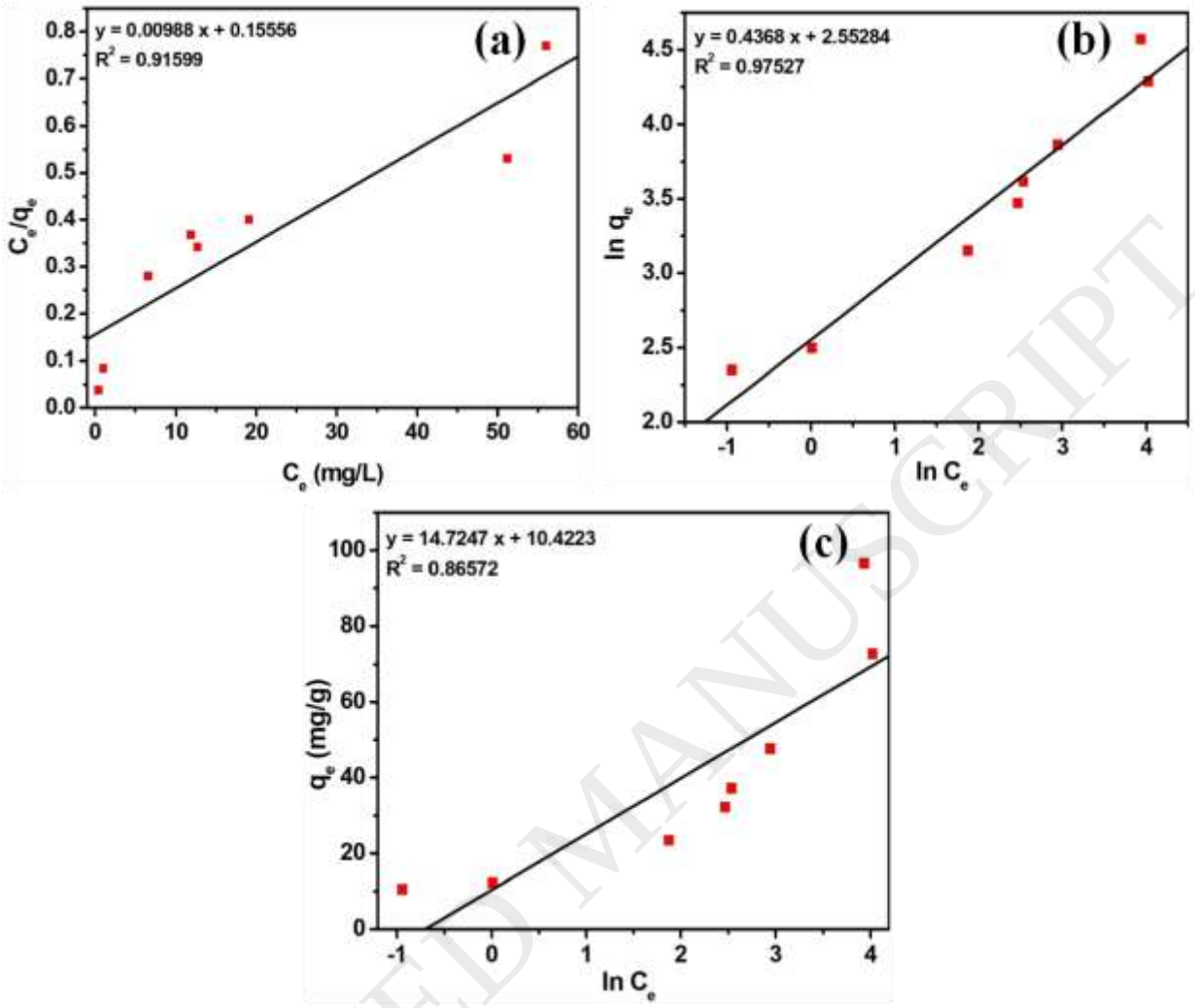

Fig. 10. (a) Langmuir, (b) Freundlich and (c) Temkin adsorption isotherm plot for the adsorption of MB over Cu-BTC.

Table 2. Isotherm parameter for the adsorption of MB dye (pH 7, temperature 298 K) on Cu-BTC in aqueous phase

Isotherm model				
Langmuir	q_L (mg/g)	b (L/mg)	R_L (Range)	R^2
	101.21	0.064	0.495-0.074	0.91599
Freundlich	K_f (mg/g)	N		R^2

	12.84	2.289		0.97527
Temkin	K_T (L/mg)	B_1	b_T (J/mol)	R^2
	2.03	14.725	168.256	0.86572

3.7. Activation energy and thermodynamic studies

The nature and adsorption behavior of MB onto Cu-BTC can be investigated by thermodynamic adsorption studies and activation energy can be calculated using Arrhenius equation:

$$\ln k_2 = \ln A - \left(\frac{E_a}{RT}\right) \quad (10)$$

where k_2 is pseudo second order rate constant, E_a is activation energy (kJ/mol), R is universal gas constant (8.314 J/mol K) and T is temperature (K). The activation energy was estimated from the slope of plot (**Fig. 11** (a)) for ln k_2 versus 1/T and results are shown in Table 3. The value of E_a gives information about the sorption process; for physisorption process, E_a value is typically lesser than 40 kJ/mol while for chemisorptions it is higher than 40 kJ/mol as leading in adsorption process [**70**]. In this study, E_a value is found to be < 40 kJ/mol thus indicates the physisorption type of adsorption. Thermodynamic parameters are considered actual indicator for describing the type and nature of adsorption process and are estimated from following equations [**71**]:

$$\ln K_C = \frac{\Delta S^O}{R} - \frac{\Delta H^O}{RT} \quad (11)$$

$$\Delta G^0 = \Delta H^0 - T\Delta S^0 \quad (12)$$

where, Kc is the distribution constant for adsorption. According to equation (12), the ΔH^0 and ΔS^0 parameters were computed by plotting graph (**Fig. 11** (b)) between ln K_c and 1/T. **Table 3** gives the thermodynamic parameters determined for MB adsorption at temperatures 298, 308, 313 K. The negative values of ΔG^0 for different temperatures signify the viability and spontaneous nature of adsorption process. The negative value of enthalpy change confirms that this work was an exothermic process [**56**]. Also negative value of ΔS^0 proposes less randomness at solid-liquid interface during adsorption and also implied that the mobility of MB onto the surface of Cu-BTC

became more controlled in contrast to that of aqueous solution. Therefore, the driving force for MB adsorption is primarily due to enthalpy effect instead of an entropy change.

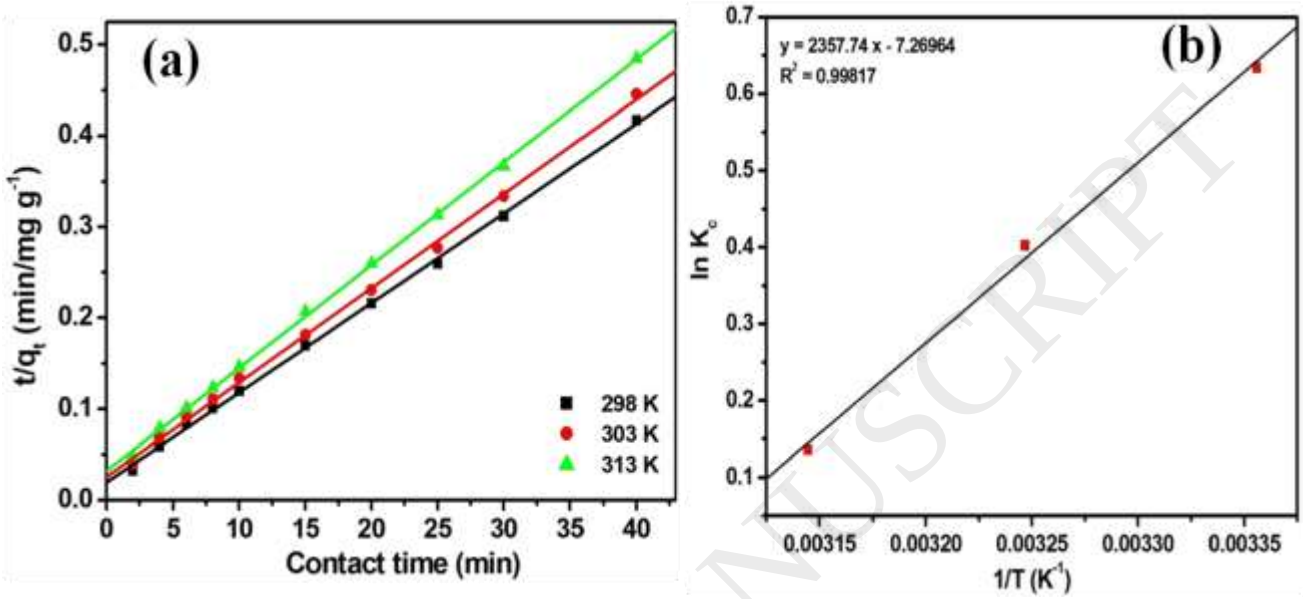

Fig. 11 (a) pseudo-second order and (b) Van't Hoff plot to get the ΔH^0 and ΔS^0 of the MB adsorption over Cu-BTC

Table 3. Thermodynamic parameters of MB adsorption over Cu-BTC at different temperatures

Methylene blue			**ΔG^0 (kJ/mol)**		
E_a, Activation energy (kJ/mol)	ΔH^0 (kJ/mol)	ΔS^0 (J/mol. K)	298 K	308 K	313K
8.404	-19.6019	-60.44	-1.6027	-0.9987	-0.6967

3.8. Reusability of Cu-BTC adsorbent

The reusability of Cu-BTC for the removal of methylene blue (200 mg/L, pH 7) was carried out by performing experiments under optimized conditions as shown in **Fig. 12**(a). The adsorption capacity of Cu-BTC declined from 96.4 to 76.2 mg/g after second cycle of adsorption. After the fourth regeneration cycle, the adsorption capacity further decreased down to 42.1 mg/g, but this is

still a good value. By comparing FTIR pattern (**Fig. 12** (b)) of synthesized and recycled Cu-BTC, slight variation between spectra was observed which indicates that dye content could be released from MB dye to Cu-BTC at room temperature. The high intensity peaks at 1640 cm^{-1} is corresponds to C=O stretching in Cu-BTC. The peaks at 1368 and 1445 cm^{-1} are assigned to C=O in the carboxylic groups. Results demonstrated that the stretching vibrations of C=O bond shifted to lesser wavenumber after adsorption as compared to synthesized Cu-BTC [**51**].

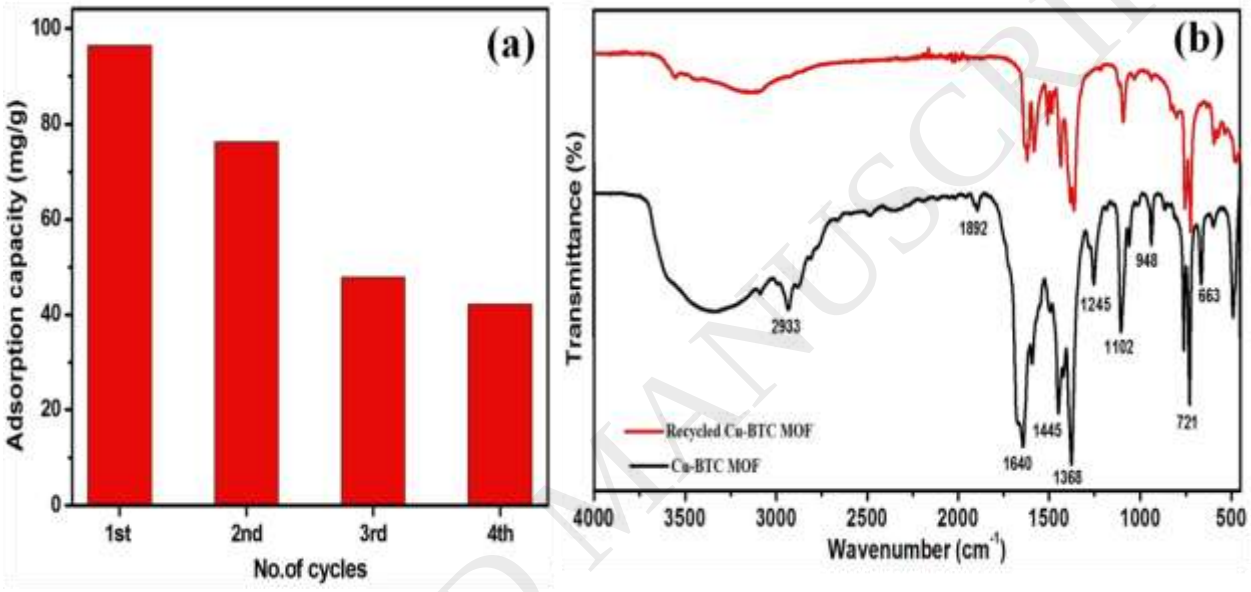

Fig. 12. (a) Reusability and (b) FTIR of as-synthesized and recycled Cu-BTC

4. Conclusions

In this work, Cu-BTC was used for the adsorptive removal of MB from wastewater. The prepared Cu-BTC MOFs exhibited octahedral shaped morphology. The kinetic data exhibited best fit with pseudo-2nd-order as compared to pseudo 1st-order-kinetic model. Adsorption isotherms were explicated by Langmuir, Freundlich and Temkin isotherms. The removal of MB dye over Cu-BTC followed Freundlich model as compared to others in terms of correlation coefficient. The thermodynamic parameters such as enthalpy (ΔH^0), entropy (ΔS^0), Gibb's free energy change (ΔG^0) were computed and it was observed that the adsorption process was impulsive and exothermic in nature. Regeneration results suggested that reused MOF can be efficiently used up

to four cycles. Therefore, by considering all the above results the Cu-BTC can be used as prominent candidate for the removal of MB dye from water.

Acknowledgement

The authors would like to acknowledge CSIR/SRF Fellowship/2016, CSIR New Delhi for providing financial support through a grant no. 09/135/0750/EMR-I and TEQIP-III grant of Dr S. S. Bhatnagar UICET, Panjab University, Chandigarh. Ahmad Umar acknowledges the Ministry of Education, Saudi Arabia for granting Promising Centre for Sensors and Electronics Devices (PCSED) to Najran University, Saudi Arabia.

References

[1]. Mingfang Yan and Zhili Li, Sci. Adv. Mater. 8, 797-803 (2016)

[2]. Shravan Pradeep, Sai Raghuram, and Sonal Mazumder, Mater. Focus 6, 657–667 (2017)

[3]. J.D. Xiao, L.G. Qiu, X. Jiang, Y.J. Zhu, S. Ye, X. Jiang, Carbon 59 (2013) 372-382.

[4] Yanqing Zhang, Yimin Zhang, Tao Liu, Zhaoquan Ai, and Shifang Yang, Sci. Adv. Mater. 9, 673–681 (2017)

[5] A. R. Cestari, E. F. S. Vieira, A. A. Pinto, E. C. N. Lopes, J. Colloid Interface Sci. 292 (2005) 363-372.

[6] Xuan Thang Cao, Dong Woo Kim, Ali Md. Showkat, Yeon Tae Jeong, and Kwon Taek Lim, Sci. Adv. Mater. 8, 322-326 (2016)

[7] B. Song, T. Wang, H. Sun, Q. Shao, J. Zhao, K. Song, L. Hao, L. Wang, Z. Guo, Dalton Trans. 46 (2017) 15769-15777.

[8] Hang Zhao, Li-Cheng Wu, and Huan-Yan Xu, Sci. Adv. Mater. 8, 1408–1416 (2016)

[9] Qi Tong, Tifeng Jiao, Haiying Guo, Jingxin Zhou, Yitian Wu, Qingrui Zhang, and Qiuming Peng, Sci. Adv. Mater. 8, 1005-1009 (2016)

[10] H. Kang, Z. Cheng, H. Lai, H. Ma, Y. Liu, X. Mai, Y. Wang, Q. Shao, L. Xiang, X. Guo, Z. Guo, Sep. Purif. Technol. 201 (2018) 193-204.

[11] Ngoc Xuan Dat Mai, Juyeon Yoon, Ji Hyeon Kim, Il Tae Kim, Hyung Bin Son, Joonwon Bae, and Jaehyun Hur, Sci. Adv. Mater. 9, 1484–1487 (2017)

[12] A. Ayar, O. Gezici, M. Küçükosmanoglu, J. Hazard. Mater. 146 (2007) 186–193.

[13] Wei Guan and Shichao Tian, Sci. Adv. Mater. 9, 1603–1609 (2017)

[14] K. Elass, A. Laachach, A. Alaoui, M. Azzi, Appl. Clay Sci. 54 (2011) 90–96.

[15] A. R. Prasad, P. R. Ammal, A. Joseph, Mater. Res. Bull. 102 (2018) 116-121.

[16] Sai Wang, Xuewen Xu, Yinghao Bai, Yuanhui Ma, Jun Zhang, Fanbing Meng, Jianling Zhao, and Chengchun Tang, Sci. Adv. Mater. 8, 1020-1027 (2016)

[17] A. Rodriguez, J. Gaarcia, G. Ovejero, M. Mestanza, J. Hazard. Mater. 172 (2009) 1311-1320.

[18] T. Wang, P. Zhao, N. Lu, H. Chen, C. Zhang, X. Hou, Chem. Eng. J. 295 (2016) 403-413.

[19] Xiaolin Hu, Jian Tian, Hongru Yang, Tong Li, Na Wei, and Hongzhi Cui, Sci. Adv. Mater. 8, 2313–2321 (2016)

[20] S. Cinar, U. H. Kaynar, T. Aydemir, S. C. Kaynar, M. Ayvacikli, Int. J. Biol. Macromol. 96 (2017) 459-465.

[21] Zhenglong Yang, Xinyan Liu, Xiaoli Xu, Sai Chen, Feng Li, Xingyi Zhu, and Yuchuan Du Sci. Adv. Mater. 8, 1901–1907 (2016)

[22] L. Zhang, M. Qin, W. Yu, Q. Zhang, H. Xie, Z. Sun, Q. Shao, X. Guo, L. Hao, Y. Zheng, Z. Guo, J. Electrochem. Soc. 164 (2017) H1086-H1090.

[23] E. Yilmaz, E. Sert, F. S. Atalay, J. Taiwan Inst. Chem. Eng. 65 (2016) 323-330.

[24] Qiongyao Zhang, Jing Xu, and Lun Luo, Sci. Adv. Mater. 9, 2082–2089 (2017)

[25] V. Gomez, M. S. Larrechi, M. P. Callao, Chemosphere 69 (2007) 1151–1158.

[26] S. Wang, Z. H. Zhu, J. Hazard. Mater. 136 (2006) 946–952.

[27] S.S. Tahir, N. Rauf, Chemosphere 63 (2006) 1842–1848.

[28] J. Huang, Y. Cao, Q. Shao, X. Peng, Z. Guo, Ind. Eng. Chem. Res. 56 (2017) 10689-10701.

[29] Fatma Yalcinkaya, Baturalp Yalcinkaya, Jakub Hruza, and Pavel Hrabak, Sci. Adv. Mater. 9, 747–757 (2017)

[30] K. Gong, Q. Hu, L. Yao, M. Li, D. Sun, Q. Shao, B. Qiu, Z. Guo, ACS Sustainable Chem. Eng. 6 (2018) 7283-7291.

[31] L. Zhang, W. Yu, C. Han, J. Guo, Q. Zhang, H. Xie, Q. Shao, Z. Sun, Z. Guo, J. Electrochem. Soc. 164 (2017) H651-H656.

[32] C. X. Yang, X. P. Yan, Anal. Chem. 83 (2011) 7144–7150.

[33] Q. Liu, L. Ning, S. Zheng, M. Tao, Y. Shi, Y. He, Sci. Rep. 3 (2013) 2916 (1-6).

[34] T. V. Vu, H. Kosslick, A. Schulz, J. Harloff, E. Paetzold, M. Schneider, J. Radnik, N. Steinfeldt, G. Fulda, U. Kragl, Appl. Catal. A. 468 (2013) 410–417.

[35] F. Wu, L. G. Qiu, F. Ke, X. Jiang, Inorg. Chem. Commun. 32 (2013) 5–8.

[36] W. Deng, T. Kang, H. Liu, J. Zhang, N. Wang, N. Lu, Y. Ma, A. Umar, Z. Guo, Sci. Adv. Mater. 10 (2018) 937-949.

[37] Y. Yin, H. Zhang, P. Huang, C. Xiang, Y. Zou, F. Xu, L. Sun, Mater. Res. Bull. 99 (2018) 152-160.

[38] Z. Wang, J. Wang, M. Li, K. Sun, C. J. Liu, Sci. Rep. 4 (2014) 5939 (1-5).

[39] F. N. Azad, M. Ghaedi, K. Dashtian, S. Hajati, V. Pezeshkpour, Ultrason. Sonochem. 31 (2016) 383-393.

[40] E. Haque, J. E. Lee, I. T. Jang, Y. K. Hwang, J. S. Chang, J. Jegal, S. H. Jhung, J. Hazard. Mater. 181 (2010) 535-542.

[41] W. Xuan, C. Zhu, Y. Liu, Y. Cui, Chem. Soc. Rev. 41 (2012) 1677–1695.

[42] Y. Ma, L. Lyu, Y. Guo, Y. Fu, Q. Shao, T. Wu, S. Guo, K. Sun, X. Guo, E. K. Wujcik, Z. Guo, Polymer 128 (2017) 12-23.

[43] Y.-P. Wang, P. Zhou, S.-Z. Luo, S. Guo, J. Lin, Q. Shao, X. Guo, Z. Liu, J. Shen, B. Wang, Z. Guo, Adv. Polym. Technol., 2018, DOI: https://doi.org/10.1002/adv.21969

[44] N. Bakhtiari, S. Azizian, J. Mol. Liq. 206 (2015) 114–118.

[45] S. S. Y. Chui, S. M. F. Lo, P. H. Charmant, A. G. Orpen, L. D. Williams, Science 283 (1999) 1148–1150.

[46] Z.-P. Wu, M.-X. Wang, L.-J. Zhou, Z.-L. Yin, J. Tan, J.-L. Zhang, Q.-Y. Chen, Trans. Nonferrous Met. Soc. China 24 (2014) 3722-3731.

[47] Q. M. Wang, D. B. Shen, M. Low, M. L. Lau, S. Deng, F. R. Fitch, N. O. Lemcoff, J. Semanscin, Micropor. Mesoporo. Mater. 55 (2002) 217-230.

[48] Y. Li, R. T. Yang, AIChE J. 54 (2008) 269-279.

[49] P. Chowdhury, C. Bikkina, D. Meister, F. Dreisbach, S. Gumma, Microporo. Mesoporo. Mater. 117 (2009) 406-413.

[50] E. Biemmi, S. Christian, N. Stock, T. Bein, Mesoporo. Mater. 117 (2009) 111-117.

[51] A. R. Abbasi, M. Karimi, K. Daasbjerg, Ultrason. Sonochem. 37 (2017) 182-191.

[52] Shan Liu, Lian-Hua Fu, Yan-Jun Liu, Ling-Yan Meng, Yan-Yan Dong, Ya-Yu Li, and Ming-Guo Ma, Sci. Adv. Mater. 8, 2045–2053 (2016)

[53] E. D. Dikio, A. M. Farah, Chem. Sci. Trans. 2 (2013) 1386-1394.

[54] S. Lin, Z. Song, G. Che, A. Ren, P. Li, C. Liu, J. Zhang, Microporo. Mesoporo. Mater. 193 (2014) 27-34

[55] J. L. C. Rowsell, O. M. Yaghi, J. Am. Chem. Soc. 128 (2006) 1304-1315.

[56] J. Lin, D. Wang, D. Chen, Q. Ge, G. Ping, M. Fan, L. Qin, K. Shu, Environ. Prog. Sustainable Energy 34 (2015) 74–80.

[57] Chencheng Wang, Feng Chen, Zhigang Chen, Chengbao Liu, Junchao Qian, Zhengyin Wu, and Zhaohou Huang, Sci. Adv. Mater. 8, 1760–1765 (2016)

[58] T. V. N. Thi, C. L. Luu, T. C. Hoang, T. Nguyen, T. H. Bui, P. H. D. Nguyen, T. P. P. Thi, Adv. Nat. Sci.: Nanosci. Nanotechnol. 4 (2013) 035016 (1-6).

[59] R. Sanz, F. Martinez, G. Orcajo, L. Wojtas and D. Briones, Dalton Trans. 42 (2013) 2392-2398.

[60] Z. Liang, M. Marshall, A. L. Chaffee, Energy Fuels 23 (2009) 2785-2789.

[61] B. H. Hameed, A. A. Ahmad, J. Hazard. Mater. 164 (2009) 870–875.

[62] M. C. Ncibi, B. Mahjoub, M. Seffen, J. Hazard. Mater. 139 (2007) 280–285.

[63] C. H. Weng, Y. F. Pan, J. Hazard. Mater. 144 (2007) 355–362.

[64] S. Eftekhari, A. Habibi-Yangjeh, Sh. Sohrabnezhad, J. Hazard. Mater. 178 (2010) 349–355.

[65] M. J. C. Calagui, D. B. Senoro, C. C. Kan, J. W. L. Salvacion, C. M. Futalan, M. W. Wan, J. Hazard. Mater. 277 (2014) 120-126.

[66] C. Djilani, R. Zaghdoudi, F. Djazi, B. Bouchekima, A. Lallam, A. Modarressi, M. Rogalski, J. Taiwan Inst. Chem. Eng. 53 (2015) 112-121.

[67] Q. Yang, Q. Zhao, S. S. Ren, Z. Chen, H. Zheng, Chem. Eng. J. 323 (2017) 74-83.

[68] W. J. Weber, J. C. Morris, J. Sanit. Eng. Div. 89 (1963) 31–60.

[69] D. Zhang, C. L. Zhang, P. Zhou, J. Hazard Mater. 186 (2011) 971-977.

[70] R. K. Gautam, S. Banerjee, M. A. Sanroman, M. C. Chattopadhyaya, J. Environ. Chem. Eng. 5 (2017) 328-340.

[71] A. Taufik, A. Muzakki, R. Saleh, Mater. Res. Bull. 99 (2018) 109-123.